Int. J. Heat Mass Transfer. Vol. 23, pp. 527–537
© Pergamon Press Ltd. 1980. Printed in Great Britain

0017–9310/80/0401–0527 $02.00/0

COMBINED HEAT AND MASS TRANSFER IN MIXED CONVECTION ALONG VERTICAL AND INCLINED PLATES

T. S. CHEN, C. F. YUH and A. MOUTSOGLOU

Department of Mechanical and Aerospace Engineering, University of Missouri-Rolla, Rolla, Missouri 65401, U.S.A.

(*Received* 3 *May* 1979 *and in revised form* 31 *October* 1979)

Abstract – An analysis is performed to study the heat- and mass-transfer characteristics of mixed convection flow along vertical and inclined flat plates under the combined buoyancy effects of thermal and mass diffusion. The analysis is for processes in which the diffusion-thermo and thermo-diffusion effects as well as the interfacial velocities due to mass diffusion are negligibly small. The plate is either maintained at a uniform temperature/concentration or subjected to a uniform heat/mass flux. Numerical results for the local Nusselt number and the local Sherwood number are presented for diffusion of common species into air and water. In general, it has been found that for the thermally assisting flow, the local surface heat- and mass-transfer rates are further enhanced when the buoyancy force from mass diffusion assists the thermal buoyancy force, but are reduced when the two buoyancy forces oppose each other. These trends are reversed for the thermally opposing flow. In addition, the effects of the combined buoyancy forces on the surface heat- and mass-transfer rates are found to diminish as the angle of inclination from the vertical increases. A comparison is also made between results from the uniform surface heat/mass flux and the uniform wall temperature/concentration.

NOMENCLATURE

C, species, mass fraction or concentration;
C_f, local friction factor;
D, binary diffusion coefficient;
f, F, reduced stream functions;
g, gravitational acceleration;
$Gr_{x,t}$, thermal Grashof number, $g\beta(T_w - T_\infty)x^3/\nu^2$;
$Gr^*_{x,t}$, modified thermal Grashof number, $g\beta q_w x^4/k\nu^2$;
$Gr_{x,c}$, Grashof number for mass diffusion, $g\beta^*(C_w - C_\infty)x^3/\nu^2$;
$Gr^*_{x,c}$, modified Grashof number for mass diffusion, $g\beta^*\dot{m}_w x^4/\rho D\nu^2$;
k, thermal conductivity of the fluid;
$\dot{m}$, mass flux of the diffusing species;
N, ratio of Grashof numbers, $Gr_{x,c}/Gr_{x,t}$;
N^*, ratio of modified Grashof numbers, $Gr^*_{x,c}/Gr^*_{x,t}$;
Nu_x, local Nusselt number, $q_w x/[(T_w - T_\infty)k]$;
Pr, Prandtl number, ν/α;
q_w, local surface heat-transfer rate per unit area;
Re_x, Reynolds number, $u_\infty x/\nu$;
Sc, Schmidt number, ν/D;
Sh_x, local Sherwood number, $\dot{m}_w x/[\rho D(C_w - C_\infty)]$;
T, fluid temperature;
u, v, velocity components in x and y directions;
x, y, axial and normal coordinates.

Greek symbols

α, thermal diffusivity of the fluid;
β, volumetric coefficient of thermal expansion, $[-(\partial\rho/\partial T)_{p,C}]/\rho$;
β^*, volumetric coefficient of expansion with mass fraction, $[-(\partial\rho/\partial C)_{p,T}]/\rho$;
γ, angle of inclination from vertical;
δ, boundary-layer thickness;
η, pseudo-similarity variable;
η_δ, dimensionless boundary-layer thickness;
θ, dimensionless temperature;
λ, dimensionless mass fraction;
μ, dynamic viscosity of the fluid;
ν, kinematic viscosity of the fluid;
ξ, thermal buoyancy force parameter, $|Gr_{x,t}|\cos\gamma/Re_x^2$;
ρ, density of the fluid;
τ, shear stress;
Φ, modified dimensionless temperature;
χ, modified thermal buoyancy parameter, $|Gr^*_{x,t}|\cos\gamma/Re_x^{5/2}$;
ψ, stream function;
ω, modified dimensionless mass fraction.

Subscripts

w, condition at the wall;
∞, condition at the free stream.

INTRODUCTION

THERMAL buoyancy effects on forced convective heat transfer over a surface may become important when the flow velocity is relatively small and the temperature difference between the surface and the ambient fluid is large. The thermal buoyancy force effects on heat-transfer characteristics of forced convection has been studied extensively for various flow configurations, particularly for forced flow along vertical and horizontal surfaces. An account of the studies for these

two flow configurations can be found, for example, in the references cited in two recent studies on the subject [1, 2]. In general, it has been found that the buoyancy force increases the rate of surface heat transfer when it assists the forced flow and decreases the heat-transfer rate when it opposes the forced flow. Very recently, Mucoglu and Chen [3] have studied the thermal buoyancy force effects on forced convection flow along inclined surfaces. They found that the effects of buoyancy forces on the wall shear and surface heat-transfer rate diminish as the angle of inclination from the vertical increases, for both assisting and opposing flows.

There are many transport processes in industry and in the environment in which buoyancy forces arise from both thermal and mass diffusion as a result of the co-existence of temperature gradients and concentration differences of dissimilar chemical species. The problems of combined buoyancy modes of thermal and mass diffusion have been studied rather extensively for laminar free convection flow along vertical and horizontal plates (see, for example [4, 5] and the references cited therein). The analysis, in general, has been based on mass diffusion processes for which very low concentration level exists, such that the diffusion-thermo and thermo-diffusion effects, along with the interfacial velocities from mass diffusion at the surface, are neglected. In their analysis on free convection flows for vertical and horizontal plates, Gebhart and Pera [4, 5] used Boussinesq approximations and presented results for air and water for Schmidt numbers of practical interest.

A survey of literature reveals that the combined effects of buoyancy forces from thermal and mass diffusion on forced convective heat and mass transfer have not been studied. Many such problems exist in engineering and environmental processes. This has motivated the present investigation. In the study, attention is directed to forced convection along vertical and inclined plates for which the plate is either maintained at a uniform temperature and concentration or subjected to a uniform surface heat and mass flux. Solutions of the transformed conservation equations are obtained by both local nonsimilarity and finite difference methods. Numerical results are presented for Prandtl numbers of 0.7 and 7 over Schmidt numbers ranging from 0.2 to 10 and from 7 to 500, respectively. These results cover a range of diffusion species of interest, respectively, for air and water.

ANALYSIS

Consider a flat plate that is inclined from the vertical with an accute angle γ, along which a forced flow moves parallel to the plate with free stream velocity u_∞, temperature T_∞, and concentration C_∞. The forced flow is above the plate when $\gamma > 0$ in the clockwise direction and below the plate when $\gamma < 0$. The plate is either maintained at a uniform temperature T_w and uniform concentration C_w or subjected to a uniform surface heat flux q_w and uniform surface mass flux $\dot{m}_w$. The streamwise coordinate x is measured from the leading edge of the plate and the transverse coordinate y is measured normal to the plate in the outward direction, for flows both above and below the plate.

By imposing the assumptions of negligible diffusion-thermo and thermo-diffusion effects, along with the Boussinesq approximations, one can write the conservation equations of the laminar boundary layer as [6]

$$\frac{\partial u}{\partial x} + \frac{\partial v}{\partial y} = 0 \tag{1}$$

$$u\frac{\partial u}{\partial x} + v\frac{\partial u}{\partial y} = \pm g\beta \sin\gamma \frac{\partial}{\partial x}\int_y^\infty (T - T_\infty)\mathrm{d}y \pm g\beta^* \sin\gamma \frac{\partial}{\partial x}\int_y^\infty (C - C_\infty)\mathrm{d}y \pm g\beta \cos\gamma (T - T_\infty) \pm g\beta^* \cos\gamma (C - C_\infty) + \nu\frac{\partial^2 u}{\partial y^2} \tag{2}$$

$$u\frac{\partial T}{\partial x} + v\frac{\partial T}{\partial y} = \alpha\frac{\partial^2 T}{\partial y^2} \tag{3}$$

$$u\frac{\partial C}{\partial x} + v\frac{\partial C}{\partial y} = D\frac{\partial^2 C}{\partial y^2} \tag{4}$$

where the conventional notations are defined in the Nomenclature. The first two terms on the RHS of equation (2) represent the streamwise pressure gradients induced by the combined buoyancy forces, with the plus and minus signs pertaining, respectively, to flows above and below the plate. The third and fourth terms denote the buoyancy forces that arise from thermal and mass diffusion, with the plus and minus signs referring, respectively, to upward and downward forced flows. Equations (1)–(4) are subjected to the following boundary conditions:

$$\begin{aligned} &u = 0, \quad v = v_w \quad \text{at } y = 0 \\ &T = T_w \quad \text{and } C = C_w \quad \text{or } q_w = -k\,\partial T/\partial y \\ &\quad \text{and } \dot{m}_w = -\rho D\,\partial C/\partial y \quad \text{at } y = 0 \\ &u \to u_\infty, \quad T \to T_\infty, \quad C \to C_\infty \quad \text{as } y \to \infty \\ &u = u_\infty, \quad T = T_\infty, \quad C = C_\infty \quad \text{at } x = 0. \end{aligned} \tag{5}$$

Equation (2) shows that both the buoyancy-induced streamwise pressure gradient terms and the buoyancy force terms exist for an inclined surface. The relative magnitude of these terms, however, depends on the angle of inclination, γ. As demonstrated in the appendix of [6], an order of magnitude analysis will lead to the result that the buoyancy-induced streamwise pressure gradient terms can be neglected in comparison with the buoyancy force terms if the condition

$$\frac{\delta}{x}\tan\gamma \ll 1 \tag{6}$$

is fulfilled. In terms of the dimensionless boundary-layer thickness η_δ (the η value for which $y = \delta$), this

condition is equivalent to

$$\tan\gamma \ll Re_x^{1/2}/\eta_\delta. \tag{7}$$

Since η_δ is about 10 and since the local Reynolds number, $Re_x = u_\infty x/\nu$, may range from 10^3 to 10^5, the values of $Re_x^{1/2}/\eta_\delta$ will lie between 3 and 30; that is, $\tan\gamma \ll 3 \sim 30$. Thus, condition (6) or (7) will be valid for angles of inclination $\gamma \ll 72° \sim 88°$ when the buoyancy-induced streamwise pressure gradient terms are neglected from equation (2). Within the framework of this approximation, the momentum equation (2) can be simplified to

$$u\frac{\partial u}{\partial x} + v\frac{\partial u}{\partial y} = \pm g\beta\cos\gamma(T-T_\infty) \pm g\beta^*\cos\gamma(C-C_\infty) + \nu\frac{\partial^2 u}{\partial y^2}. \tag{8}$$

The conservation equations for the problem under study can then be described by equations (1), (3)–(5), (8), subject to the condition given by equation (6) or (7). It is noted here that for $\gamma = 0°$, equation (8) with $\cos\gamma = 1$ represents exactly the complete x-momentum equation for a vertical plate without any approximations. This can also be seen from equation (2) by putting $\gamma = 0°$. To obtain solutions of the governing system of equations, these equations are first transformed into a dimensionless form, as described in the following.

Uniform wall temperature/concentration (UWT/UWC) case

Let the pseudo-similarity variable η and the x-dependent dimensionless coordinate $\xi(x)$ that represents the thermal buoyancy effect be

$$\eta = y(u_\infty/\nu x)^{1/2}, \qquad \xi = \xi(x) \tag{9}$$

and introduce the reduced stream function $f(\xi,\eta)$, the dimensionless temperature $\theta(\xi,\eta)$, and the concentration ratio $\lambda(\xi,\eta)$ as

$$f(\xi,\eta) = \psi(x,y)/(\nu u_\infty x)^{1/2} \tag{10}$$

$$\theta(\xi,\eta) = (T-T_\infty)/(T_w-T_\infty),$$
$$\lambda(\xi,\eta) = (C-C_\infty)/(C_w-C_\infty) \tag{11}$$

where the stream function $\psi(x,y)$ satisfies the mass conservation equation (1) with

$$u = \partial\psi/\partial y, \qquad v = -\partial\psi/\partial x. \tag{12}$$

Next, by introducing equations (9)–(12) into equations (8) and (3)–(5), one arrives at the following system of equations

$$f''' + \tfrac{1}{2}ff'' \pm \xi(\theta + N\lambda) = \xi(f'\,\partial f'/\partial\xi - f''\,\partial f/\partial\xi) \tag{13}$$

$$\frac{\theta''}{Pr} + \tfrac{1}{2}f\theta' = \xi(f'\,\partial\theta/\partial\xi - \theta'\,\partial f/\partial\xi) \tag{14}$$

$$\frac{\lambda''}{Sc} + \tfrac{1}{2}f\lambda' = \xi(f'\,\partial\lambda/\partial\xi - \lambda'\,\partial f/\partial\xi) \tag{15}$$

$$f(\xi,0) = 0, \quad f'(\xi,0) = 0$$
$$\theta(\xi,0) = \lambda(\xi,0) = 1 \tag{16}$$
$$f'(\xi,\infty) = 1, \quad \theta(\xi,\infty) = \lambda(\xi,\infty) = 0$$

where the primes stand for partial derivatives with respect to η, Pr is the Prandtl number, Sc is the Schmidt number, the thermal buoyancy force parameter $\xi(x)$ is given by

$$\xi = |Gr_{x,t}|\cos\gamma/Re_x^2 \tag{17}$$

and

$$N = \beta^*(C_w-C_\infty)/\beta(T_w-T_\infty) = Gr_{x,c}/Gr_{x,t} \tag{18}$$

with

$$Gr_{x,t} = g\beta(T_w-T_\infty)x^3/\nu^2,$$
$$Gr_{x,c} = g\beta^*(C_w-C_\infty)x^3/\nu^2 \tag{19}$$

denoting the local Grashof numbers for thermal and mass diffusion, respectively.

The quantity ξ is a measure of the thermal buoyancy force effect on forced convection and N is a measure of the relative effects between buoyancy forces that arise from mass diffusion and thermal diffusion. Since ξ denotes magnitude, it is noted that the plus and minus signs appearing on the LHS of equation (13) pertain to thermal buoyancy force assisting the forced flow ($Gr_{x,t}\cos\gamma/Re_x^2 > 0$) and opposing the forced flow ($Gr_{x,t}\cos\gamma/Re_x^2 < 0$), respectively. The buoyancy force due to concentration difference assists the thermal buoyancy force, i.e. the two buoyancy forces act in the same direction, when $N > 0$. On the other hand, they act in the opposite directions when $N < 0$. The situation in which there is no buoyancy force effect from mass diffusion corresponds to $N = 0$.

It must be mentioned that in writing the condition $f(\xi,0) = 0$ in equation (16), the normal velocity at the wall v_w associated with the mass diffusion process has been neglected. This results from the assumption of a very low concentration level in the diffusion process. The condition for the neglect of v_w can be found as

$$2\frac{v_w x}{\nu}Re_x^{-1/2} \ll 1 \tag{20}$$

or

$$\frac{2}{Sc}(C_w-C_\infty)[-\lambda'(0)] \ll 1 \tag{21}$$

when use is made of Fick's law.

Some of the physical quantities of interest include the local friction factor C_f, the local Nusselt number Nu_x, and the local Sherwood number Sh_x. They are defined, respectively, by

$$C_f = \frac{\tau_w}{\rho u_\infty^2/2}, \qquad Nu_x = \frac{q_w}{T_w-T_\infty}\frac{x}{k},$$
$$Sh_x = \frac{\dot{m}_w}{C_w-C_\infty}\frac{x}{\rho D}. \tag{22}$$

By employing the definitions of wall shear stress $\tau_w = \mu(\partial u/\partial y)_{y=0}$, along with Fourier's law $q_w =$

$-k(\partial T/\partial y)_{y=0}$ and Fick's law $\dot{m}_w = -\rho D(\partial C/\partial y)_{y=0}$, it can be shown that

$$C_f Re_x^{1/2} = 2f''(\xi,0) \tag{23}$$

$$\begin{aligned} Nu_x Re_x^{-1/2} &= -\theta'(\xi,0), \\ Sh_x Re_x^{-1/2} &= -\lambda'(\xi,0). \end{aligned} \tag{24}$$

Uniform surface heat/mass flux (UHF/UMF) case

The nonsimilarity variables for this case are

$$\eta = y(u_\infty/\nu x)^{1/2}, \quad \chi = \chi(x) \tag{25}$$

and the dimensionless stream function, temperature, and concentration are defined by

$$F(\chi,\eta) = \psi(x,y)/(\nu u_\infty x)^{1/2} \tag{26}$$

$$\begin{aligned} \Phi(\chi,\eta) &= (T-T_\infty)Re_x^{1/2}/(q_w x/k), \\ \omega(\chi,\eta) &= (C-C_\infty)Re_x^{1/2}/(\dot{m}_w x/\rho D) \end{aligned} \tag{27}$$

Substituting equations (25–27) into equations (8) and (3)–(5), one obtains

$$F''' + \tfrac{1}{2}FF'' \pm \chi(\Phi + N^*\omega) = \tfrac{3}{2}\chi(F'\,\partial F'/\partial\chi - F''\,\partial F/\partial\chi) \tag{28}$$

$$\frac{\Phi''}{Pr} + \tfrac{1}{2}F\Phi' - \tfrac{1}{2}F'\Phi = \tfrac{3}{2}\chi(F'\,\partial\Phi/\partial\chi - \Phi'\,\partial F/\partial\chi) \tag{29}$$

$$\frac{\omega''}{Sc} + \tfrac{1}{2}F\omega' - \tfrac{1}{2}F'\omega = \tfrac{3}{2}\chi(F'\,\partial\omega/\partial\chi - \omega'\,\partial F/\partial\chi) \tag{30}$$

$$\begin{aligned} F(\chi,0) = 0, \quad F'(\chi,0) = 0, \\ \Phi'(\chi,0) = \omega'(\chi,0) = -1 \end{aligned} \tag{31}$$

$$F'(\chi,\infty) = 1, \quad \Phi(\chi,\infty) = \omega(\chi,\infty) = 0$$

where the thermal buoyancy parameter χ has the expression

$$\chi = |Gr_{x,t}^*|\cos\gamma/Re_x^{5/2} \tag{32}$$

and the quantity

$$N^* = (\dot{m}_w\beta^*/\rho D)/(q_w\beta/k) = Gr_{x,c}^*/Gr_{x,t}^* \tag{33}$$

measures the relative effect of buoyancy forces between mass and thermal diffusion. The modified local Grashof numbers for thermal and mass diffusion are given, respectively, by

$$\begin{aligned} Gr_{x,t}^* &= g\beta q_w x^4/k\nu^2, \\ Gr_{x,c}^* &= g\beta^*\dot{m}_w x^4/\rho D\nu^2. \end{aligned} \tag{34}$$

The plus and minus signs appearing in front of χ on the LHS of equation (28) refer, respectively, to thermal buoyancy assisting ($Gr_{x,t}^*\cos\gamma/Re_x^{5/2} > 0$) and opposing ($Gr_{x,t}^*\cos\gamma/Re_x^{5/2} < 0$) the forced flow. There is no buoyancy effect from mass diffusion when $N^* = 0$. Both thermal buoyancy force and buoyancy force due to concentration difference act in the same direction when $N^* > 0$, whereas they act in the opposite directions when $N^* < 0$.

As in the case of uniform wall temperature and uniform wall concentration, the interfacial velocity at the wall, v_w, due to mass diffusion process has been neglected in arriving at the condition $F(\chi,0) = 0$ in equation (31). This approximation is valid when the condition

$$2\frac{v_w x}{\nu}Re_x^{-1/2} \ll 1 \quad \text{or} \quad \frac{2}{Sc}\frac{C_w - C_\infty}{\omega(\chi,0)} \ll 1 \tag{35}$$

is fulfilled.

The local friction factor, the local Nusselt number, and the local Sherwood number as defined by equation (22) now have the expressions

$$C_f Re_x^{1/2} = 2F''(\chi,0) \tag{36}$$

$$\begin{aligned} Nu_x Re_x^{-1/2} &= 1/\Phi(\chi,0), \\ Sh_x Re_x^{-1/2} &= 1/\omega(\chi,0). \end{aligned} \tag{37}$$

Comparisons between UWT/UWC and UHF/UMF cases

A direct comparison of the local Nusselt numbers between the uniform wall temperature/concentration (UWT/UWC) case and the uniform surface heat/mass flux (UHF/UMF) case is of practical interest. This will be done later when the numerical results are presented. To facilitate such a comparison, it is necessary to define an equivalent thermal buoyancy force parameter ξ_e for the UHF case in terms of the local wall temperature $T_w(x)$ such that

$$\xi_e = |(Gr_{x,t})_e|\cos\gamma/Re_x^2 \tag{38}$$

where

$$(Gr_{x,t})_e = g\beta[T_w(x) - T_\infty]x^3/\nu^2 \tag{39}$$

and

$$T_w(x) - T_\infty = (q_w x/k)Re_x^{-1/2}\Phi(\chi,0) \tag{40}$$

from the Φ expression in equation (27). Substituting equation (40) into equation (38) and making use of equation (32), one obtains

$$\xi_e = \chi\Phi(\chi,0). \tag{41}$$

For $\xi = \chi\Phi(\chi,0)$, one can find the Nusselt number ratio between the UHF and UWT cases by employing the Nu_x expressions in equations (24) and (37) as

$$(Nu_x)_{\text{UHF}}/(Nu_x)_{\text{UWT}} = -1/[\Phi(\chi,0)\theta'(\xi,0)]. \tag{42}$$

Similarly, one can determine the Sherwood number ratio by defining an equivalent buoyancy force parameter due to mass diffusion for the uniform surface mass flux (UMF) case in terms of the local wall mass concentration $C_w(x)$ as

$$\xi_{c,e} = |(Gr_{x,c})_e|\cos\gamma/Re_x^2 = N\xi_e \tag{43}$$

where

$$(Gr_{x,c})_e = g\beta^*[C_w(x) - C_\infty]x^3/\nu^2 \tag{44}$$

and

$$C_w(x) - C_\infty = \dot{m}_w(x/\rho D)Re_x^{-1/2}\omega(\chi,0) \tag{45}$$

from equation (27). Substitution of equation (45) into equation (43) along with the use of equation (32) results in

$$\xi_{c,e} = N^*\chi\omega(\chi,0) \tag{46}$$

For $\xi_c = N^*\chi\omega(\chi,0)$, one finds from the Sh_x expressions in equations (24) and (37) that

$$(Sh_x)_{UMF}/(Sh_x)_{UWC} = -1/[\omega(\chi,0)\lambda'(\xi,0)]. \tag{47}$$

Since $\Phi(\chi,0)$ and $\omega(\chi,0)$ depend on N^*, and since $\theta'(\xi,0)$ and $\lambda'(\xi,0)$ depend on N, a relationship between N^* and N needs to be determined before the $(Nu_x)_{UHF}/(Nu_x)_{UWT}$ ratio or the $(Sh_x)_{UMF}/(Sh_x)_{UWC}$ ratio can be evaluated. This relationship can be determined from equations (41), (43), and (46) as

$$N^*/N = \Phi(\chi,0)/\omega(\chi,0) \tag{48}$$

when $\xi = \xi_e$. In addition, it can be seen that equation (46) reduces to equation (41). When $Sc = Pr$, one can observe from equations (29) and (30) that $\Phi(\chi,0) = \omega(\chi,0)$. This leads to $N^* = N$ from equation (48). In the same manner, a comparison between equations (14) and (15) shows that $\lambda'(\xi,0) = \theta'(\xi,0)$ when $Sc = Pr$. It can therefore be concluded that the $(Sh_x)_{UMF}/(Sh_x)_{UWC}$ ratio is exactly identical to the $(Nu_x)_{UHF}/(Nu_x)_{UWT}$ ratio when $Sc = Pr$ and hence $N^* = N$ under the equivalent buoyancy force parameter $\xi = \xi_e$.

NUMERICAL SOLUTIONS

Equations (13)–(15) for the uniform wall temperature/concentration (UWT/UWC) case and (28)–(30) for the uniform surface heat/mass flux (UHF/UMF) case are partial differential equations that are coupled, respectively, through the functions f, θ, λ and F, Φ, ω for the respective parametric values of N, Pr, Sc, and N^*, Pr, Sc. In the present investigation, these equations subject to their respective boundary conditions, equations (16) and (31), were solved either by the local nonsimilarity method (see, for example, [2, 3, 7]) or by a finite-difference method similar to, but modified from that given in [8]. The former method was used in the UWT/UWC case for $Pr = 0.7$ and the latter method in the UWT/UWC case for $Pr = 7$ and in the UHF/UMF case for both $Pr = 0.7$ and 7. In the local nonsimilarity method, the solutions were truncated at the second level, because it has been established from previous studies that this level provides results that are very accurate for all practical purposes. In the present study, the resulting equations were solved by the Runge–Kutta integration scheme, along with the Newton–Raphson shooting method to refine the initial values at $\eta = 0$ until the conditions at the edge of the boundary layers (i.e. at $\eta = \eta_\delta$) were satisfied simultaneously within a tolerance of 10^{-5} or smaller. In the computations, the maximum η_δ values ranged from 8 to 15 as the Schmidt number decreased from 10 to 0.2. The step size $\Delta\eta$ was varied from 0.02 for $0 \le \eta \le 4$ to 0.04 for $\eta > 4$, which was found to be adequate for providing accurate numerical results.

For the case of $Pr = 7$ (i.e. diffusion of species into water), the Schmidt numbers of practical interest lie about 500 and the mass-fraction boundary-layer thickness is very small ($\eta_\delta < 1$) as compared to the flow and thermal boundary-layer thicknesses. Because of the high Schmidt numbers involved, the numerical integration solution becomes difficult to obtain and time consuming. It was then decided to solve the system of equations (13)–(16) for the case of UWT/UWC with $Pr = 7$ and the system of equations (28)–(30) for the case of UHF/UMF with $Pr = 0.7$ and 7 by a finite-difference method. This solution procedure is well documented and can be found, for example, in [8]. In this method, an η_δ value of 10 was found to be sufficient for all Schmidt numbers ranging from 7 to 500 and a step size of 0.02 was sufficient for $Sc = 7$. However, the step size for $Sc = 100$ and 500 had to be varied from 0.005 for $0 \le \eta \le 1$ to 0.020 for $1 \le \eta \le 5$ to 0.040 for $5 \le \eta \le 10$ for the UWT/UWC case and varied from 0.002 for $0 \le \eta \le 0.5$ to 0.02 for $0.5 \le \eta \le 5$ to 0.04 for $5 \le \eta \le 10$ for the UHF/UMF case. This is because a very small step size is required inside the mass-fraction boundary layer ($\eta < 1$) in order to provide accurate numerical results. On the other hand, a step size of $\Delta\xi = 0.25$ or $\Delta\chi = 0.2$ was found to be adequate for the ξ or χ variable.

In the computations for the UWT/UWC case, the values of $Gr_{x,t}\cos\gamma/Re_x^2$ ranged from -0.5 to 2.0 and the N values from -1.0 to 2.0 for both $Pr = 0.7$ and 7. For the UHF/UMF case, the values of $Gr^*_{x,t}\cos\gamma/Re_x^{5/2}$ ranged from -0.5 to 2 and the N^* values ranged from -1.0 to 2.0. The Schmidt number range for $Pr = 0.7$ covers diffusion of gases or vapors into air, such as hydrogen ($Sc = 0.22$), water vapor (0.60), ammonia (0.78), carbon dioxide (0.94), methanol (0.97), ethyl alcohol (1.30), benzene (1.76), ethyl benzene (2.01), and naphthalene (2.57). The Schmidt number of 500 for $Pr = 7$ covers closely the diffusion into water of ammonia ($Sc = 455$), carbon dioxide (453), nitrogen (468), sulfur dioxide (523), methanol (556), sodium chloride (580), and chlorine (617).

RESULTS AND DISCUSSION

The variations of the local Nusselt number Nu_x and the local Sherwood number Sh_x with the thermal buoyancy force parameter $Gr_{x,t}\cos\gamma/Re_x^2$ for the uniform wall temperature/concentration (UWT/UWC) case are shown, respectively, in Figs. 1 and 2 for $Pr = 0.7$, with values of N ranging from -1.0 to 2.0 and Schmidt numbers from 0.2 to 10. The corresponding results for $Pr = 7$ are shown, respectively, in Figs. 3 and 4 with N values from -1.0 to 2.0 and Schmidt numbers of 7, 100 and 500. Similar graphs for the uniform surface heat/mass flux (UHF/UMF) case are plotted against the thermal buoyancy force parameter $Gr^*_{x,t}\cos\gamma/Re_x^{5/2}$, respectively, in Figs. 5 and 6 for $Pr = 0.7$, with N^* values from -1.0 to 2.0 and Schmidt numbers from 0.6 to 1.0, and in Figs. 7 and 8 for $Pr = 7$, with N^* values of -1.0 to 2.0 and Sc values of 7, 100 and 500. These figures for $Pr = 0.7$ then show the results for diffusion of some typical gases or vapors into

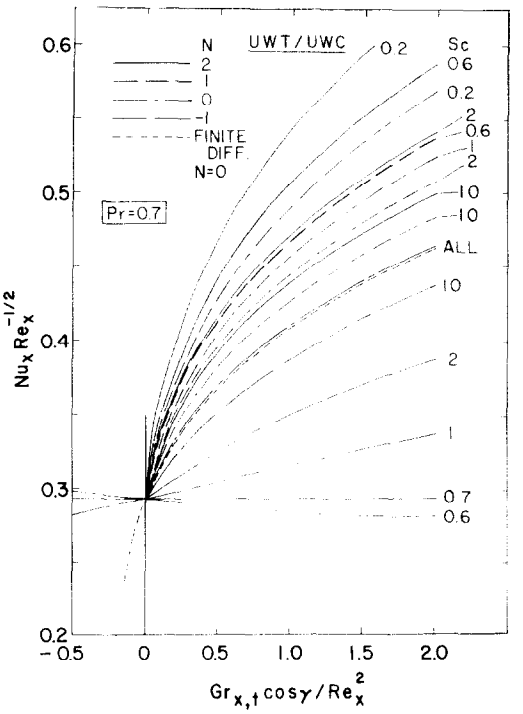

FIG. 1. Local Nusselt number results for uniform wall temperature/concentration, $Pr = 0.7$.

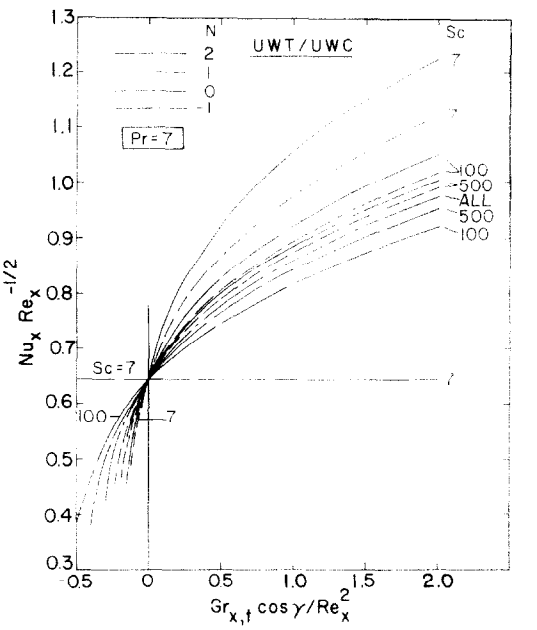

FIG. 3. Local Nusselt number results for uniform wall temperature/concentration, $Pr = 7$.

fluids with $Pr = 0.7$ (such as air) and those for $Pr = 7$ illustrate the results for diffusion of some typical species into fluids with $Pr = 7$ (such as water). To conserve space, the results for the local friction factor are not illustrated. As mentioned earlier, the results for the UWT/UWC case with $Pr = 0.7$ were obtained from solutions by the local nonsimilarity method, whereas those for the UWT/UWC case with $Pr = 7$ and the UHF/UMF case with $Pr = 0.7$ and 7 were from the finite-difference method of solution. For the UWT/UWC case with $Pr = 0.7$, the results from the finite-difference solution for $N = 0$ are also shown in Fig. 1 for comparisons with those from the local

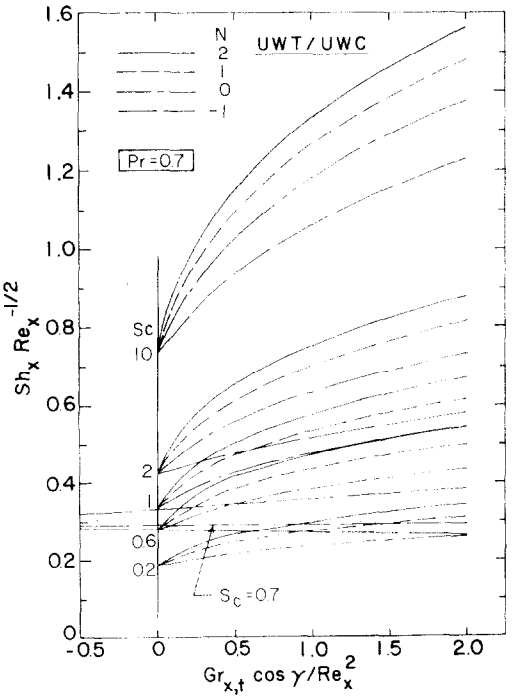

FIG. 2. Local Sherwood number results for uniform wall temperature/concentration, $Pr = 0.7$.

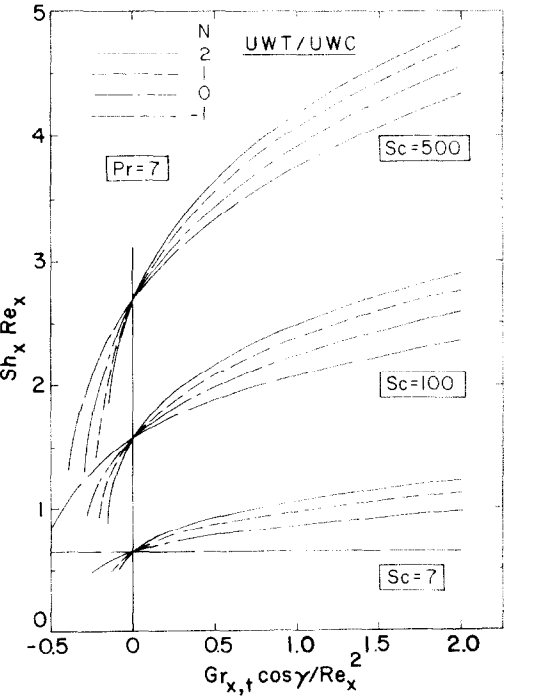

FIG. 4. Local Sherwood number results for uniform wall temperature/concentration, $Pr = 7$.

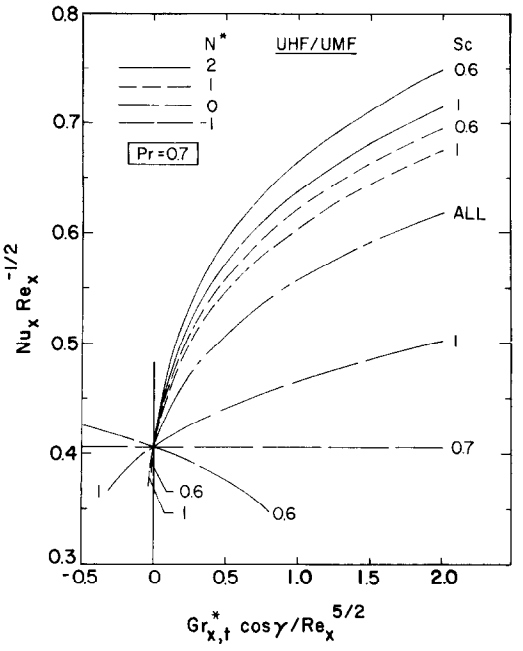

FIG. 5. Local Nusselt number results for uniform surface heat/mass flux, $Pr = 0.7$.

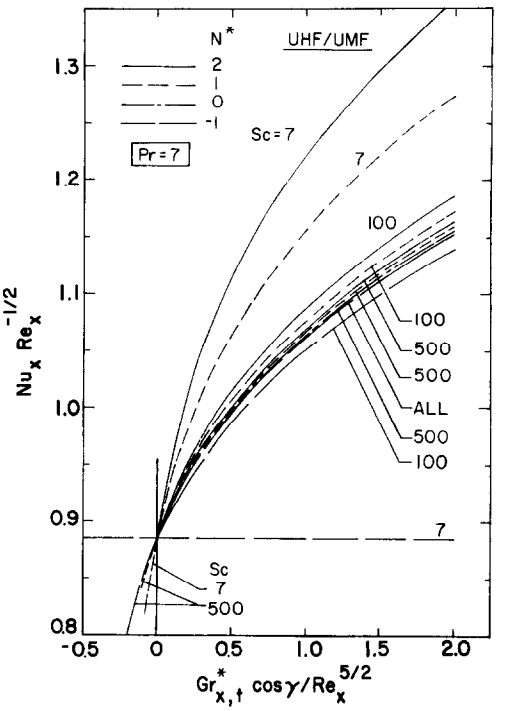

FIG. 7. Local Nusselt number results for uniform surface heat/mass flux, $Pr = 7$.

nonsimilarity solution. A close agreement between the two sets of results serves to verify the accuracy of the local nonsimilarity method of solution.

To explain the Nu_x and Sh_x results shown in Figs. 1–4 for the UWT/UWC case and in Figs. 5–8 for the UHF/UMF case, attention is first directed to the curves for $N = 0$ and $N^* = 0$; that is, to the curves for the case in which the buoyancy force arises solely from the temperature differences in the fluid and there exists no buoyancy force effect from concentration differences. It is seen from these figures that for $N = 0$ (or $N^* = 0$) the local Nusselt number and the local Sherwood number increase with increasing thermal buoyancy force intensity for assisting flow ($Gr_{x,t} \cos\gamma/Re_x^2 > 0$ or $Gr^*_{x,t} \cos\gamma/Re_x^{5/2} > 0$) and decrease with

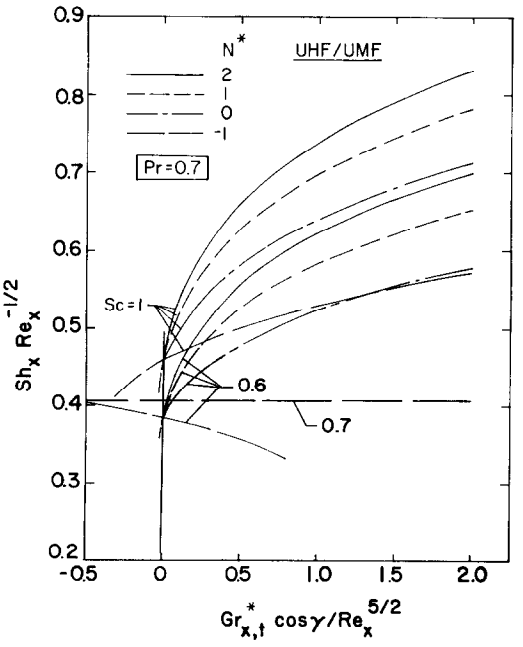

FIG. 6. Local Sherwood number results for uniform surface heat/mass flux, $Pr = 0.7$.

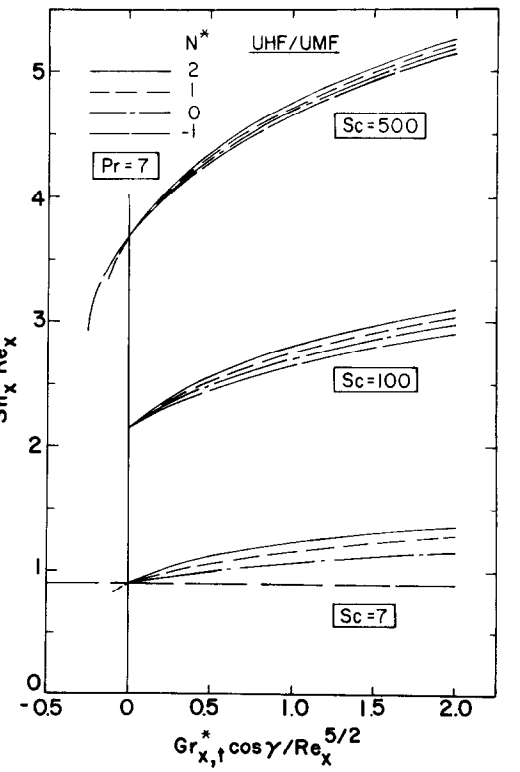

FIG. 8. Local Sherwood number results for uniform surface heat/mass flux, $Pr = 7$.

increasing thermal buoyancy force intensity for opposing flow ($Gr_{x,t}\cos\gamma/Re_x^2 < 0$ or $Gr^*_{x,t}\cos\gamma/Re_x^{5/2} < 0$). When $N > 0$ (or $N^* > 0$), that is, when the buoyancy force from mass diffusion acts in the same direction as the thermal buoyancy force, these quantities are further enhanced or reduced as compared to their respective values for $N = 0$ (or $N^* = 0$), depending on whether the thermal buoyancy force assists or opposes the forced flow. These trends are reversed when $N < 0$ (or $N^* < 0$), that is, when the buoyancy force from mass diffusion acts in the opposite direction to the thermal buoyancy force. In addition, it is seen that for $N > 0$ (or $N^* > 0$), the surface heat- and mass-transfer rates increase and decrease with increasing thermal buoyancy force, respectively, for thermally assisting and opposing flows. However, for $N = -1.0$ (or $N^* = -1.0$), while the same trends are seen to prevail when $Sc > Pr$, they are reversed when $Sc < Pr$. This bahavior is due to the net buoyancy force effect from thermal and mass diffusion and needs further explanation.

From Figs. 1–4 one can see that the local Nusselt and Sherwood numbers are independent of $Gr_{x,t}\cos\gamma/Re_x^2$ when $N = -1.0$ and $Sc = Pr$. These quantities are also independent of $Gr^*_{x,t}\cos\gamma/Re_x^{5/2}$ when $N^* = -1.0$ and $Sc = Pr$ (see Figs. 5–8). This is because the θ and λ or Φ and ω solutions are identical when $Sc = Pr$ [see equations (14) and (15) or (29) and (30)] and, in addition, with $N = -1.0$ the term $\pm\xi(\theta + N\lambda)$ in equation (13) or with $N^* = -1$ the term $\pm\chi(\Phi + N^*\omega)$ in equation (28) becomes zero, signifying that the combined net buoyancy force effect from thermal and mass diffusion is zero, that is, the two buoyancy forces are of the same intensity but are exactly opposite in their directions of action. The resulting situation is exactly identical to that for pure forced convection. When $Sc < Pr$ and $N = -1.0$ in the uniform wall temperature/concentration case, such as $Sc = 0.6$, $Pr = 0.7$, and $N = -1.0$ in Figs. 1 and 2, the values of Nu_x and Sh_x *decrease* with increasing values of $Gr_{x,t}\cos\gamma/Re_x^2 > 0$ and *increase* with increasing value of $Gr_{x,t}\cos\gamma/Re_x^2 < 0$, because the term $(\theta + N\lambda)$ becomes negative. In fact, these trends will exist for any combination of $N < 0$, Sc, and Pr as long as $(\theta + N\lambda)$ remains negative. This same behavior is also true for the uniform surface heat/mass flux case when $Sc < Pr$ and $N^* = -1.0$.

The behaviors of Nu_x and Sh_x with the changes in N and $Gr_{x,t}\cos\gamma/Re_x^2$ (or N^* and $Gr^*_{x,t}\cos\gamma/Re_x^{5/2}$) are in conformity with the physical situations, as is to be expected. For both $N > 0$ and $N < 0$ (or $N^* > 0$ and $N^* < 0$), larger departures of the Nu_x values from those of $N = 0$ (or $N^* = 0$) are associated with smaller values of the Schmidt number, for both positive and negative values of $Gr_{x,t}\cos\gamma/Re_x^2$ (or $Gr^*_{x,t}\cos\gamma/Re_x^{5/2}$). The reason for this is that a diffusing species with a smaller Schmidt number has a larger binary diffusion coefficient which will then exert a larger effect on the flow and thermal fields. On the other hand, larger values of Sherwood number are associated with larger values of the Schmidt numbers. This is because an increase in the Schmidt number implies a decrease in the binary diffusion coefficient for a given fluid and a decrease in the concentration boundary-layer thickness relative to the flow boundary-layer thickness. For $Sc > 1$, the concentration boundary-layer thickness becomes smaller than the flow boundary-layer thickness, thus resulting in a larger mass fraction gradient at the wall. As the Schmidt number increases further, the mass fraction gradient at the wall (see Fig. 11) and hence the Sherwood number increases accordingly. Although not illustrated, it is stated here that the behavior of the local friction factor results parallels that of the local Nusselt number results.

The Nu_x and Sh_x results presented in Figs. 1–8 reduce to those for a vertical plate when the angle of inclination from the vertical γ is zero. Since $\zeta_{\text{inclined plate}}/\zeta_{\text{vertical plate}} = \chi_{\text{inclined plate}}/\chi_{\text{vertical plate}} = \cos\gamma$, it can be seen that the thermal buoyancy force effects on Nu_x and Sh_x diminish as γ increases. Thus, to induce the same effect on the Nu_x and Sh_x at a given angle $\gamma > 0$ as at $\gamma = 0$, it is necessary to increase the thermal buoyancy force intensity $Gr_{x,t}/Re_x^2$ or $Gr^*_{x,t}/Re_x^{5/2}$ by a factor of $1/\cos\gamma$.

Representative velocity, temperature, and mass-fraction profiles are illustrated only for the uniform wall temperature/concentration case with $Pr = 0.7$, respectively, in Figs. 9–11. To preserve the clarity of the figures, curves are shown only for $Gr_{x,t}\cos\gamma/$

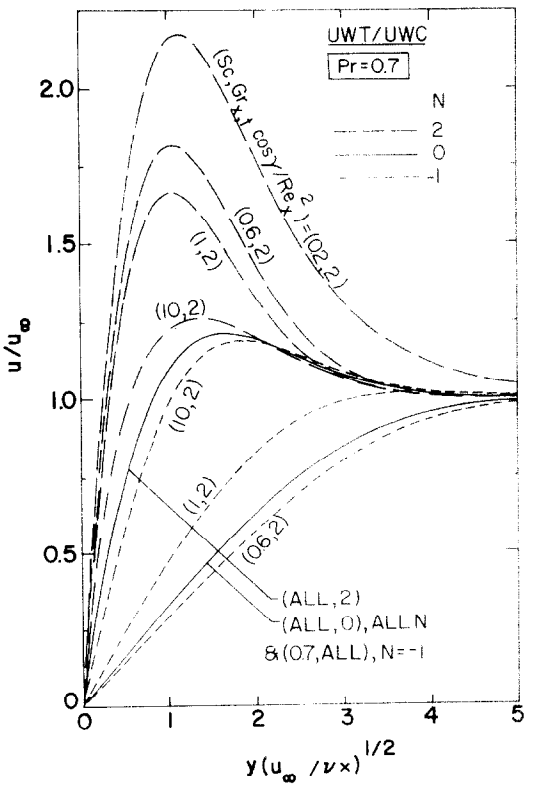

FIG. 9. Representative velocity profiles for uniform wall temperature/concentration, $Pr = 0.7$.

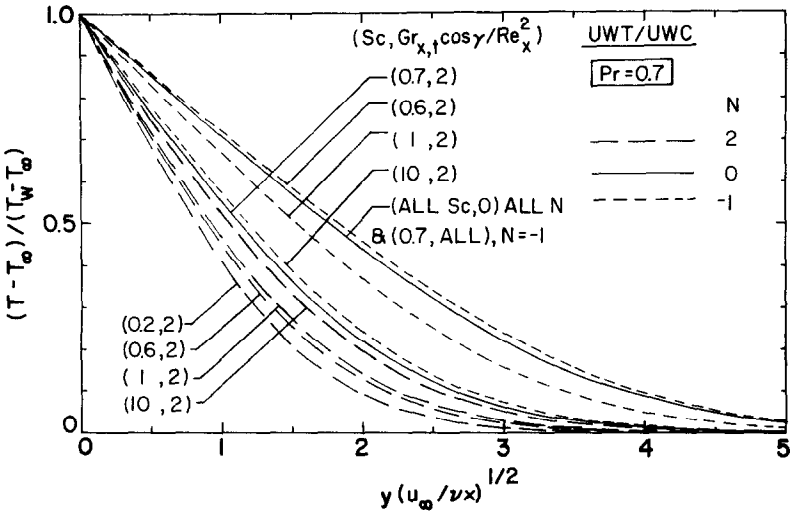

FIG. 10. Representative temperature profiles for uniform wall temperature/concentration, $Pr = 0.7$.

$Re_x^2 = 0$, 2 and $N = -1.0$, 0, 2.0 for several typical Schmidt numbers. The curves for $Gr_{x,t}\cos\gamma/Re_x^2 = 0$ correspond to pure forced convection, so are the curves for $N = -1.0$ with $Sc = Pr$, as was explained in the discussion of the Nu_x and Sh_x results. The velocity profiles (Fig. 9) show that if the combined effects of $Gr_{x,t}\cos\gamma/Re_x^2$ and N result in a net buoyancy force that assists the forced flow, the velocity gradient at the wall increases beyond that for pure forced convection. This net effect is seen to increase with increasing value of N for a given Schmidt number and with decreasing Schmidt number for a given N value, particularly when N is large and Sc is small, as evidenced from an accompanying rapid increase in the velocity near the wall and an overshooting of the velocity beyond its free stream value inside the flow boundary layer. On the other hand, when the net effect of thermal and concentration buoyancy forces contributes to an opposing flow, both the velocity and the velocity gradient at the wall are reduced as compared to those for pure forced convection (see the curve for $Sc = 0.6$, $Gr_{x,t}\cos\gamma/Re_x^2 = 2$, $N = -1.0$ in Fig. 9).

With respect to the temperature profiles (Fig. 10), the temperature gradient at the wall is seen to increase as N increases or as Sc decreases when the net buoyancy force effect of thermal and mass diffusion results in an assisting flow. The opposite trend is observed when the net buoyancy force effect gives rise to an opposing flow (see the curve for $Sc = 0.6$, $N = -1.0$, and $Gr_{x,t}\cos\gamma/Re_x^2 = 2$ in Fig. 10). Thus, the effects of $Gr_{x,t}\cos\gamma/Re_x^2$, N, and Sc on the thermal field are similar to those on the flow field. Although not shown, it is noted here that fluids with $Pr = 7$ provide, under the same values of N, Sc, and $Gr_{x,t}\cos\gamma/Re_x^2$, larger temperature gradients at the wall than fluids with $Pr = 0.7$. The mass-fraction profiles (Fig. 11) exhibit trends that are somewhat different from those of the velocity and temperature profiles. While the

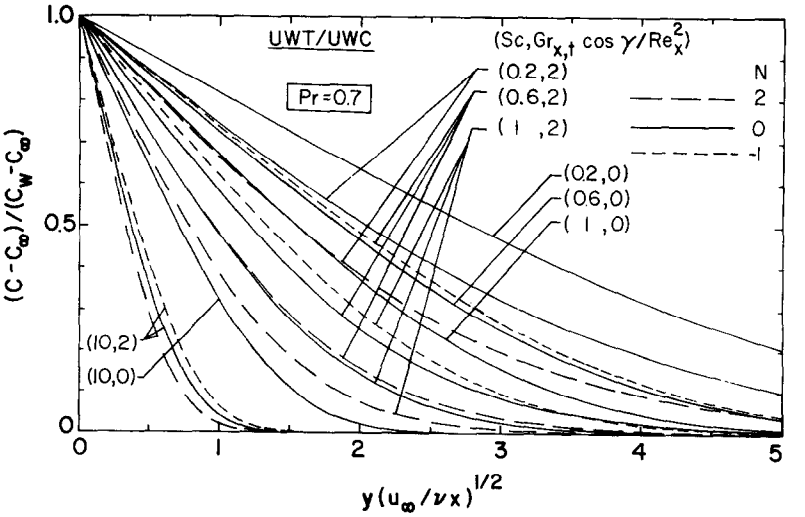

FIG. 11. Representative mass fraction profiles for uniform wall temperature/concentration, $Pr = 0.7$.

concentration gradient at the wall is seen to increase with increasing value of N when the net buoyancy force effect is to assist the forced flow, a larger increase is accompanied by a larger Schmidt number. This behavior, similar to the effect of Prandtl number on the temperature profiles, was explained when the Sherwood number results were discussed.

Finally, the local Nusselt numbers between the UHF/UMF case and the UWT/UWC case are compared in Fig. 12, in which the $(Nu_x)_{UHF}/(Nu_x)_{UWT}$ ratio is plotted against the equivalent buoyancy force parameter $(Gr_{x,t})_e \cos\gamma/Re_x^2$. Curves are shown only for the cases of $Sc = Pr$ and $N^* = N$. It can be seen from the figure that for an equivalent thermal buoyancy force parameter as defined by equation (41), the Nusselt number ratio is larger than one; that is, the Nusselt numbers for the uniform surface heat/mass flux case are larger than those for the uniform wall temperature/concentration case. In addition, it is seen that the Nusselt number ratio for $Pr = Sc = 0.7$ is larger than that for $Pr = Sc = 7$, and that this ratio decreases with an increasing value of N for a given buoyancy force intensity. Furthermore, the $(Nu_x)_{UHF}$ $(Nu_x)_{UWT}$ ratios decrease as $(Gr_{x,t})_e \cos\gamma/Re_x^2$ increases and become essentially constant for large values of $(Gr_{x,t})_e \cos\gamma/Re_x^2$. For the case of $N = N^* = -1.0$ and $Pr = Sc$, the Nusselt number ratios do not depend on $(Gr_{x,t})_e \cos\gamma/Re_x^2$ because of the zero net buoyancy force under these conditions. The curves in Fig. 12 are also applicable exactly as the Sherwood number ratio, $(Sh_x)_{UMF}/(Sh_x)_{UWC}$, because they are for $Sc = Pr$ and $N^* = N$ under $\xi = \xi_e$, as was explained in the Analysis section.

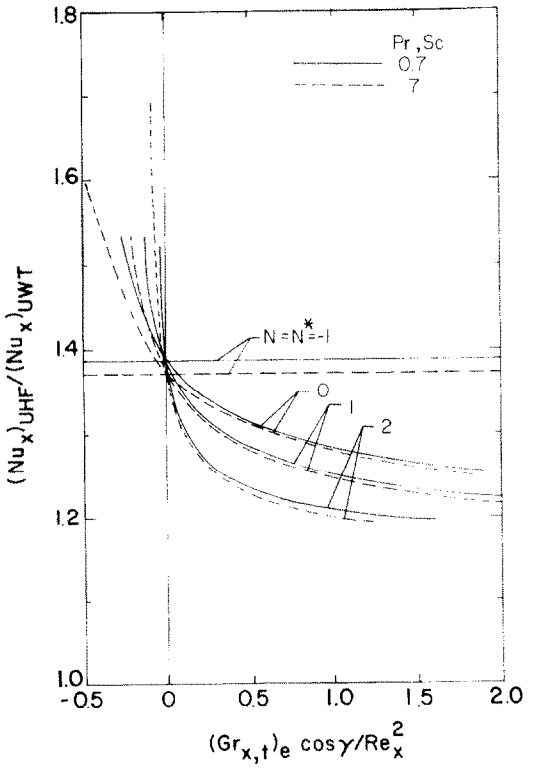

FIG. 12. The Nusselt number ratio $(Nu_x)_{UHF}/(Nu_x)_{UWT}$ and the Sherwood number ratio $(Sh_x)_{UMF}/(Sh_x)_{UMC}$ for $Sc = Pr$ and $N^* = N$.

CONCLUSIONS

From the present study of mixed convection on vertical and inclined plates with combined buoyancy force effects of thermal and mass diffusion, it has been found in general that for both uniform wall temperature/concentration and uniform surface heat/mass flux cases, the local friction factor, the local Nusselt number, and the local Sherwood number increase when the net effect of the combined buoyancy forces assists the forced flow and decrease when the net effect opposes the forced flow. The combined buoyancy force effects on these three quantities are enhanced when the buoyancy force from mass diffusion assists the thermal buoyancy force and are reduced when they oppose each other. In addition, a smaller Schmidt number is found to exert a larger effect on the friction factor and the Nusselt number, whereas a larger Schmidt number is responsible for a larger effect on the Sherwood number. The buoyancy force effect diminishes as the angle of inclination from the vertical increases. In addition, combined heat and mass transfer under uniform surface heat/mass flux provides larger local Nusselt and Sherwood numbers than the combined transfer under uniform wall temperature/concentration.

Acknowledgement – The present study was supported by a grant from the National Science Foundation (NSF ENG 75-15033 A01).

REFERENCES

1. P. H. Oosthuizen and R. Hart, A numerical study of laminar combined convective flow over flat plates, *J. Heat Transfer* **95C**, 60–63 (1973).
2. T. S. Chen, E. M. Sparrow and A. Mucoglu, Mixed convection in boundary layer flow on a horizontal plate, *J. Heat Transfer* **99C**, 66–71 (1977).
3. A. Mucoglu and T. S. Chen, Mixed convection on inclined surfaces, *J. Heat Transfer* **101C**, 422–426 (1979).
4. B. Gebhart and L. Pera, The nature of vertical natural convection flows resulting from the combined buoyancy effects of thermal and mass diffusion, *Int. J. Heat Mass Transfer* **14**, 2025–2050 (1971).
5. L. Pera and B. Gebhart, Natural convection flows adjacent to horizontal surfaces resulting from the combined buoyancy effects of thermal and mass diffusion, *Int. J. Heat Mass Transfer* **15**, 269–278 (1972).
6. T. S. Chen and C. F. Yuh, Combined heat and mass transfer in natural convection on inclined surfaces, *Numer. Heat Transfer* **2**, 233–250 (1979).
7. T. S. Chen and A. Mucoglu, Buoyancy effects on forced convection along a vertical cylinder, *J. Heat Transfer* **97C**, 198–203 (1975).
8. T. Cebeci and P. Bradshaw, *Momentum Transfer in Boundary Layers*, Chapter 7. Hemisphere, Washington, D.C. (1977).

TRANSFERT DE CHALEUR ET DE MASSE EN CONVECTION MIXTE LE LONG DE PLAQUES VERTICALES OU INCLINEES

Résumé — On étudie les caractéristiques du transfert de chaleur et de masse en convection mixte le long de plaques planes verticales ou inclinées, sous l'influence des diffusions de chaleur et de masse. On suppose que la thermodiffusion ainsi que les vitesses interfaciales sont négligeables. La plaque est maintenue soit à température ou concentration uniforme soit encore à flux massique ou thermique uniforme. On présente des résultats numériques pour le nombre de Nusselt local et le nombre de Sherwood local pour la diffusion d'espèces courantes dans l'air et l'eau. On trouve que les flux surfaciques locaux sont augmentés lorsque les forces dues à la diffusion massique assistent celles dues à la diffusion thermique, mais sont réduits quand ces forces s'opposent. De plus, les effets combinés des forces sur les flux surfaciques de masse et de chaleur diminuent lorsque l'angle d'inclinaison par rapport à la verticale augmentent. On fait une comparaison entre les résultats relatifs au flux uniforme de chaleur ou de masse et ceux relatifs à la température ou concentration uniforme.

GLEICHZEITIGER WÄRME- UND STOFFÜBERGANG BEI GEMISCHTER KONVEKTION LÄNGS VERTIKALER UND GENEIGTER PLATTEN

Zusammenfassung—Eine Analyse wird durchgeführt, um die Eigenschaften des Wärme- und Stoffübergangs von gemischter Konvektionsströmung entlang vertikaler und geneigter ebener Platten unter den gleichzeitigen Einflüssen der Auftriebskräfte von Wärmeleitung und Diffusion zu untersuchen. Die Analyse gilt für Prozesse, bei denen sowohl die Diffusionsthermo- und Thermodiffusionseffekte als auch die Grenzflächengeschwindigkeiten infolge der Stoffdiffusion vernachlässigbar klein sind. Die Platte wird entweder auf gleichmäßiger Temperatur bzw. Konzentration gehalten oder einer gleichmäßigen Wärme- bzw. Massenstromdichte unterworfen. Zahlenmäßige Ergebnisse für die örtliche Nusselt-Zahl und die ortliche Sherwood-Zahl werden für die Diffusion bekannter Stoffe in Luft und Wasser angegeben. Ganz allgemein wurde gefunden, daß bei thermisch unterstützter Strömung die örtlichen Wärme- und Stoffübergangswerte an der Wand weiter vergrößert werden, wenn die Auftriebskraft infolge von Stoffdiffusion die thermische Auftriebskraft verstärkt, jedoch reduziert werden, wenn die Auftriebskräfte entgegengerichtet sind. Diese Trends werden bei thermisch behinderter Strömung umgekehrt. Außerdem wurde festgestellt, daß sich die Wirkungen der kombinierten Auftriebskräfte auf die Wärme- bzw. Stoffübergangswerte an der Oberfläche mit zunehmendem Neigungswinkel, bezogen auf die der Vertikalen, vermindern. Es werden auch die Ergebnisse für gleichförmige Wärme- bzw. Massenstromdichte an der Oberfläche mit denen für gleichmäßige Temperatur bzw. Konzentration verglichen.

СОВМЕСТНЫЙ ТЕПЛО- И МАССОПЕРЕНОС ПРИ СМЕШАННОЙ КОНВЕКЦИИ НА ВЕРТИКАЛЬНЫХ НАКЛОННЫХ ПЛАСТИНАХ

Аннотация — Проведен анализ тепло- и массообменных характеристик конвективного течения вдоль вертикальных и наклонных плоских пластин при совместном действии подъёмных сил, обусловленных диффузией тепла и массы. Анализ выполнен для процессов, в которых диффузионный термоэффект и термодиффузионный эффект, а также величина скорости на пластине, обусловленная диффузией массы, пренебрежимо малы. Пластина или находится при однородной температуре–концентрации или подвержена действию однородного теплового–массового потока. Для диффузии обычных веществ в воздухе и воде даны численные значения локального числа Нуссельта и локального числа Шервуда. Найдено, что тепловая скорость локального тепло- и массопереноса на поверхности возрастает, если подъёмная сила, обусловленная диффузией массы, направлена в сторону действия подъёмной силы, обусловленной диффузией тепла, и уменьшается, если эти силы противоположно направлены. Обратное влияние наблюдается в случае, если тепловая подъёмная сила противоположна течению. Кроме того найдено, что совместное влияние подъёмных сил на скорость тепло- и массопереноса на поверхности уменьшается по мере увеличения угла наклона. Проведено сравнение результатов, полученных при однородном потоке тепла–массы на поверхности и при однородной температуре–концентрации потока на стенке.